

Accepted on 21 March 2001 for publication in
the Astrophysical Journal

THE STRUCTURE AND MOTIONS OF THE 3C 120 RADIO JET ON SCALES OF 0.6 TO 300 PARSECS

R. C. Walker, J. M. Benson

National Radio Astronomy Observatory¹, Socorro, NM 87801

`cwalker@nrao.edu, jbenson@nrao.edu`

S. C. Unwin

Jet Propulsion Laboratory, Pasadena, CA, 91109

`unwin@huey.jpl.nasa.gov`

M. B. Lystrup²

Portland State University, Portland, OR, 97207

`lystrup@physics.ucdavis.edu`

T. R. Hunter

Harvard-Smithsonian Center for Astrophysics, Cambridge, MA, 02138

`thunter@cfa.harvard.edu`

G. Pilbratt

ESA Astrophysics Division/Space Science Department, Noordwijk, The Netherlands

`gpilbratt@astro.estec.esa.nl`

P. E. Hardee

Department of Physics & Astronomy, The University of Alabama, Tuscaloosa, AL 35487

`hardee@athena.astr.ua.edu`

ABSTRACT

Results are presented from long term VLBI monitoring of the parsec-scale radio jet in 3C 120 at 5 and 1.7 GHz. The 5 GHz sequence includes a few early epochs at 10.7 GHz. Superluminal features are seen leaving the core at intervals of less than a year, about as often as new features could be distinguished with the 0.6 parsec resolution of the observations. The underlying jet is continuous, but not smooth, and the measured features are simply the bright points in the convolution of the observing beam with brightness fluctuations that occur on many scales. The velocity of different features varies, but not by more than about a factor of 2. Clear variations in the velocity of an individual feature are not seen. Some features that were observed leaving the core in the 5 GHz observations with 0.6 pc resolution are followed at 1.7 GHz, with 2.4 pc resolution, to projected distances in excess of 25 pc from the core. Older features up to at least 150 pc in projection from the core are still moving at superluminal apparent speeds and are therefore presumed to be relativistic. Beyond that, the data are inadequate for motion measurements. The region where the jet slows to non-relativistic speeds has not been found.

There are suggestions of stationary features, or brightening and dimming regions, through which the moving features pass. These may be locations where there is interaction with the external medium, or they may simply be the result of variations in the jet angle to the line-of-sight. The observation of stationary features in an otherwise moving jet reinforces the idea that the lack of motion of the knot at 4'' (2 kpc), that has been found not to be superluminal in other observations, might not actually imply that the jet has slowed by that position. The structure of the jet in the vicinity of the most likely stationary feature is suggestive of a helical pattern seen in projection. The deprojected wavelength of the pattern is very long relative to the jet radius, unlike the situation in sources such as M87 (Owen et al. 1989). If the 3C 120 jet does contain a slowly-moving, helical structure, then theory suggests that the jet resides in a relatively cool medium, not in a relativistically hot cocoon or lobe.

Subject headings: galaxies: individual (3C 120) — galaxies:jets — galaxies: active — radio continuum: galaxies — hydrodynamics — relativity

¹The National Radio Astronomy Observatory is a facility of the National Science Foundation, operated under cooperative agreement by Associated Universities, Inc.

²Current address: University of California Davis, Davis, California, 95616

1. Introduction

The radio source 3C 120 exhibits structure on all scales from under a parsec to hundreds of kiloparsecs (Walker, Benson, & Unwin 1987). It is dominated by a variable core that is resolved with Very Long Baseline Interferometry (VLBI). A prominent one-sided jet is seen extending from the core on subparsec scales to about a hundred kiloparsecs. On the largest scales there is a complex, two-sided lobe structure extending to about $14'$, or about half a megaparsec for $z = 0.033$ (Baldwin et al. 1980) and $H_0 = 75 \text{ km s}^{-1}\text{Mpc}^{-1}$, the value that will be used in this paper (this gives a scale of 0.60 pc mas^{-1}). Superluminal motion is observed in the jet which, because of the low redshift, can be studied with greater linear resolution than most other extragalactic superluminal sources. This was one of the first 4 sources in which superluminal motions were found in the early 1970s and it has been studied with VLBI extensively ever since (Sielstad et al. 1979; Walker et al. 1982; Benson et al. 1988; Gómez et al. 2000, and references therein). The standard model for superluminal motion involves relativistic motions in a jet oriented nearly along the line-of-sight (Blandford & Königl 1979).

The central region of the 3C 120 host galaxy is a strong and variable emitter of radiation at all observed frequencies. Because of the presence of broad emission lines, the galaxy is usually classified as a Seyfert 1 (Burbidge 1967), although its properties are also consistent with those of a broad line radio galaxy and, to some extent, a low luminosity quasar. The galaxy is of order an arcminute in size, with extensive H II regions that may be ionized by the nucleus (Baldwin et al. 1980). Its morphology does not clearly match either a spiral or an elliptical, and may be the disturbed product of a merger (Moles et al. 1988). Maraschi et al. (1991) give broadband spectra from infrared to X-rays and report on monitoring observations over much of this range. There is a pronounced and variable UV excess which they model with a face-on accretion disk that feeds a $4 \times 10^7 M_\odot$ black hole at a variable rate of somewhat under a solar mass per year. At optical wavelengths, variability is observed in both the continuum (Lyutyi 1979; Wlerick, Westerlund, & Garnier 1979; Pollock et al. 1979) and the spectral lines (Oke, Readhead, & Sargent 1980; Peterson et al. 1998). Reverberation mapping techniques have been used to derive a mass for the central black hole of about $3 \times 10^7 M_\odot$ (Wandel, Peterson, & Malkan 1999). 3C 120 is a complex and variable X-ray source with the unusual property that the spectral index varies with the intensity (Halpern 1985; Maraschi et al. 1991). Grandi et al. (1997) find X-ray properties similar to those of a radio quiet Seyfert, including the presence of strong iron lines, indicating that beamed emission does not dominate at these frequencies.

The radio jet is among the few that is seen at other wavelengths. An optical counterpart, extending out to $15''$, was reported by Hjorth et al. (1995). The radio-to-optical spectral index is 0.65, about the same as the radio spectral index on the same scales. In addition, there is an X-ray emission knot that is coincident with the $20''$ radio knot and is probably explained by synchrotron emission (Harris et al. 1999).

Recent high frequency VLBI observations at 86, 43 and 22 GHz (Gómez et al. 1998; Gómez,

Marscher, & Alberdi 1999; Gómez et al. 2000) have produced high resolution images and a 16-month movie of the innermost features of the jet. The 86 GHz Coordinated Millimeter VLBI Array observations put an upper limit on the core size of 0.033 pc; the core size lies below the resolution of the 86 GHz image which is $54\mu\text{as}$. The 43 and 22 GHz observations, made with the National Radio Astronomy Observatory's (NRAO) Very Long Baseline Array (VLBA), show that the inner jet structure is complex and exhibits superluminal motions on very small scales. The movie shows evidence for interaction with a cloud of density and core distance intermediate between typical broad and narrow line clouds. The complexity of the structure at high resolution makes it clear that features in lower resolution observations, such as those presented in this paper, are likely to be blends of smaller scale components. The 43 and 22 GHz observations show that the linear polarization on small scales is variable with some features near the core having magnetic fields across the jet. Polarization percentages of up to 10% are seen, increasing with core distance. Farther from the core, and at much larger scales observed with the VLA (Walker, Benson, & Unwin 1987), the polarization indicates that the magnetic fields are parallel to the jet. VLBA measurements made in 1996 showed upper limits to circular polarization of about 0.2% (Homan & Wardle 1999).

Recent studies have begun to apply physical models of jets to observations of 3C 120. The jet shows a variety of knots and side-to-side structures, some reminiscent of helical structures. Hydrodynamical jet theories incorporating shocks have been used to model the moving knots in superluminal sources (Gómez et al. 1997, and references therein). It has been suggested that the motion of the inner jet structure 3C 120 may be described in this way (Gómez et al. 1998). Both moving and stationary features can be accommodated in such models. Helical patterns are expected for some types of jet instabilities (Hardee 1987, 2000, and references therein). The superluminal motion along a curved trajectory seen in the radio source 3C 345 can be explained by helical jet models (Hardee 1987; Owen et al. 1989; Steffen et al. 1995).

According to the standard model, the observation of superluminal motions is good evidence that a jet is relativistic. The fact that a large proportion of bright, compact radio sources show superluminal motions suggests that many jets are relativistic on parsec scales, although there are selection effects due to relativistic beaming. It is not clear how far from the core the jets remain relativistic. At larger core distances, they become broader and features are larger, so measurement of small angular velocities is more difficult. Because of its close proximity, 3C 120 has high angular rates of motion compared to other superluminal sources making it a prime candidate for attempts to find motions at large angular distances from the core. So far superluminal motion has been seen in the source to distances of tens of parsecs (Benson et al. 1988). On arc second scales, a radio knot in the jet $4''$ from the core has been shown to have an upper limit on its motions of significantly smaller than the speed of light (Muxlow & Wilkinson 1991; Walker 1997). This might suggest that the jet has slowed, or moved out of the line-of-sight, by that distance. But the knot could be a stationary feature, perhaps a shock or bend, in a jet that is still relativistic. This possibility is supported by the fact that the large scale structure is two sided, but the jet is still very one sided on the scale of the knot, suggesting that the emission is still beamed on that scale. It is also supported

by optical line observations of regions on both sides of the nucleus that show evidence of interaction with the jet (Hua 1988; Axon et al. 1989). One of the goals of the 1.7 GHz observations presented here is to look for motions on scales intermediate between those usually probed with VLBI and the larger scale structures studied with linked interferometers.

In this paper we present the results obtained from five epochs of 1.7 GHz ($\lambda=18$ cm) VLBI observations spanning from 1982 to 1997. We also present 5 GHz ($\lambda=6$ cm) VLBI monitoring data which was taken approximately three times per year from 1977 through 1988. A few of the early observations of this sequence were made at 10.7 GHz. With this long series of observations, we can attempt to discern how frequently new components appear, what sort of trajectory they follow, and whether the velocities are constant for a given feature and between features. At 1.7 GHz, the core is not as dominant as at higher frequencies and a wealth of jet structure is observable up to about half an arcsecond from the core.

2. The Observations

2.1. Monitoring at 5 GHz

Between 1977 and 1988, 3C 120 was observed approximately 3 times per year with VLBI. Until 1981, the observations alternated between 10.7 GHz and 5 GHz. After 1981, it was realized that the motions in the source were sufficiently fast that the interval between same-frequency observations was too long to follow features unambiguously. After that date, nearly all observations were made at 5 GHz. For this paper, the 10.7 GHz images have been convolved to the same resolution as the 5 GHz observations and used as part of the 5 GHz monitoring sequence.

The early observations used the main antennas of the U.S. VLBI Network. As the years progressed, so did the size of the arrays as more U.S. antennas and, especially, as European antennas were added. The first observations involved only 3 antennas. By the time the series was terminated, a typical observation involved 11 antennas. All of these observations used the Mark II VLBI recording system, with a 2 MHz bandwidth and 1 bit sampling (Clark 1973). Correlation was done on one of the NRAO 3 station correlator, the Caltech 5 station correlator, or the Caltech Block II (16 Mark II stations) correlator, depending on epoch. Results up to 1980.27 were reported by Walker et al. (1982). This paper will not consider the first few observations because of their low quality, but will include observations after 1978.91 in the analysis, even though the first few of those were previously reported. The antennas involved in both these observations and in the 1.7 GHz observations described below are listed in Table 1. The date, frequency, antennas, and image peak flux density per beam for each of the observations at 5 or 10.7 GHz are listed in Table 2.

The 5 and 10.7 GHz observations were calibrated and imaged using standard procedures using either the Caltech VLBI package or AIPS at near the time of the observations. The flux scales are usually based on antenna temperatures measured at one or more of Effelsberg, Green Bank, and

Owens Valley. They are probably good to about 10% in most cases. However at least one image (1983.25) seems to have an inconsistent flux density scale relative to the others; the measured fluxes are low. Perhaps this is because that epoch did not include any short baselines. No attempt at correction has been made, partly for lack of an obvious way to determine a correction. But the dip in fluxes at that time should not be believed.

The images, consisting of CLEAN components convolved with a common restoring beam of 7.0×1.0 mas in position angle -10° , are shown in Figures 1 to 3. The extremely elongated beam is the result of the the low declination of the source (5°) and fact that nearly all of the antennas available at the time lay along a NE/SW line from Europe to California. For most epochs, the residuals are not included, but this does not make a significant difference at the contour levels used. Some of the more recent images do include the residuals. The quality of the images improved over the years, as is reflected in the differing lowest contour level displayed in each of the figures.

Figure 4 shows the component motions. A straight slice was made in position angle -105° along the ridge line of the jet in each of the images. The parts of that slice that appear to be reliable for identification of features were fit using between 2 and 6 Gaussian components. In Figure 4, the amplitudes along each slice are displayed as the width of the shaded structure centered at the date of observation. The fitted Gaussians were used to produce a model for the amplitudes along the slice. This model is shown as the thin lines that appear to outline each of the shaded regions. The fact that the lines appear to outline the shading, rather than either having shading extend outside the lines, or having white space inside the lines, indicates that the Gaussian fits produce a good description of the slice data. Note that the lines only extend over the region where structures are thought to be reasonably reliable, the region over which the fits were made. Especially in some of the earliest, and least reliable epochs, the fits were not extended over all regions that seem to show emission. The fitted position of each component is marked along with an error bar. For the core, that error bar is the maximum of the formal fit error for that component and a somewhat arbitrary minimum error of 0.3 mas meant to account for alignment uncertainties as discussed below. For other features, the error is the geometric sum of the core error and the formal fit errors for the component position. For the stronger features, the errors are dominated by the assumed alignment uncertainty. Thus the error bars are meant reflect the full uncertainty of the position of each component.

The slices have been aligned by shifting each one so that the position of the easternmost Gaussian, which is presumed to represent the core, is set at zero offset. Therefore the positions of other components are relative to the core. Some such alignment scheme is required because, without use of phase calibration using a reference source, there is no absolute position information available. But no alignment scheme will be perfect. The apparent core position can be influenced by emerging jet components while they are still too close to be resolved from the core. Such a component would shift the apparent core toward the jet, which would make the apparent distance to other jet features smaller. The apparent core position can also be influenced by variations in the length of the optically thick region at the base of the jet. This region is expected to be shorter at

higher frequencies so the distance to jet features is likely to be higher when measured at 10.7 GHz rather than 5.0 GHz. Examination of Figure 4 shows that the alignment would not be significantly different if it were based on an assumption of linear motions of jet components. This suggests that the apparent core position does not vary significantly. Estimating by eye, the core position probably does not vary by more than about 0.3 mas, and that value is used as the minimum core position error.

Most of the components whose positions are shown in Figure 4 are marked as belonging to a specific feature seen at multiple epochs and labeled with a letter. Such components are marked with closed circles. Components marked with open circles in Figure 4 are not included in any motion analysis. The positions of all components belonging to each moving feature were fit, in a least squares sense, for a feature angular speed and a start date. Straight lines indicating the fitted motion are drawn on the figure. The rates for each feature, along with the formal fit errors, are displayed on the figure. The fit results, including the start dates, are also given in Table 4. The errors on the start date are not symmetric. Typically the uncertainty extends significantly farther toward earlier than toward later times. The quoted errors were determined by exploring Chi-squared as a function of the start date. None of the error bars should be taken too seriously. They are correct under the assumptions that the motion is linear, that the decomposition of the structure into Gaussian components is appropriate, and that the images are reliable even in the regions of relatively weak emission. It is unclear how to incorporate uncertainties related to these assumptions, but a reasonable guess would be that they double the possible rate errors.

It has been noted that, especially during the period between 1981.63 and 1984.40 when the observations occurred at very regular intervals, there is a possible aliasing or “stroboscopic” effect. The data could be explained in terms of features moving toward the core or even by features moving outward at about 3 times the apparent rate. The position fits for such cases are not as good as for the unaliased outward motion and the apparent expansion of the outer envelope of observed emission is not as easily understood. But such cases are not excluded. However at other times, especially late in the project, the spacing of epochs was not so regular and it is reasonably clear that such a stroboscopic effect is not happening. Also the assumed direction and rates are consistent with the 1.7 GHz results presented below and with the high-resolution, frequent-sampling results of Gómez et al. (2000), both of which are much less subject to such effects.

There is what appears to be a gap in the monitoring of features at 5 GHz at the beginning of 1986. That is the result of a couple of circumstances. First, that time was preceded by a period of very low activity in the source so there were no features along the jet with any significant brightness. Second, the core flared at that time, starting new features, but also making it harder to see any more distant features. Finally, due to scheduling and processing problems, there is a full year with no observations. As a result of these factors, the monitoring effectively started from scratch after 1986.

2.2. Observations at 1.7 GHz

There have been 5 VLBI observations of 3C 120 at 1.7 GHz as summarized in Table 3. Images from the first two have been published in Benson et al. (1988), although they were remade with more modern imaging methods, such as the use of robust weighting (Briggs 1995), for this paper. All of these observations involved a large number of antennas. However the low declination of the source, combined with the wide longitude range of the antennas, makes the coverage of the (u,v) plane rather poor, especially for the longer baselines. The beams are not as seriously elongated as at 5 GHz because antennas off the NE/SW line were recruited. But other holes in the coverage remain. See the plots in Benson et al. (1988) for examples. The first 3 observations used the Mark II VLBI system with 2 MHz bandwidth and 1 bit sampling. The 1982.78 data were correlated on the Caltech 5 station correlator. The 1984.26 data were correlated on the NRAO 3 station correlator as part of what has since become known as the “World Radio Array” set of observations of 4 sources. The 1989.85 data were correlated on the Caltech Block II correlator. The final two epochs were recorded on the much wider bandwidth VLBA and Mark IV recording systems. The 1994.44 observation was made with just the 10 antennas of the VLBA (Napier et al. 1994) using a total of 32 MHz bandwidth and 1 bit sampling. The 1997.71 data used a global array and both VLBA and Mark IV recording systems. The total bandwidth was again 32 MHz, but this time 2 bit samples were used. Both the 1994.44 and 1997.71 observations were correlated on the VLBA correlator. The improvement of data quality with the wider bandwidth systems and the better (u,v) coverage of the VLBA is readily apparent in the images.

The 1.7 GHz images are displayed on 3 different scales in Figures 5, 6, and 7. Figure 5 shows images from the two wide bandwidth observations over the full region in which emission was detected. That region extends to about $0''.5$. These images were made with tapered data to give relatively low resolution to help draw out the larger scale structure. The beam was 18×13 mas at position angle 3° . These images show that the jet is a continuous structure from the core region to at least a $0''.5$. In fact, it is known to be a continuous structure from milliarcseconds to about $14''$ (Walker, Benson, & Unwin 1987). The current images show much more clearly than before that the jet has a smooth envelope; the edges follow smooth curves. However, there is considerable structure in the emission internal to the jet, with significant side-to-side variations and pronounced knots along the jet.

Figure 6 shows all 5 epochs with a window that includes everything out to 360 mas, including the big bulge at a bit over 200 mas. All images have been made using a Gaussian restoring beam of 10×4 mas FWHM elongated in a position angle of -10° . Note that the larger scale regions are much smoother in the recent images than in the ones based on the older Mark II data. This is not a real effect in the source, but a reflection of the behavior of the CLEAN deconvolution algorithm when dealing with a combination of lower signal-to-noise ratio data, poorer (u,v) coverage (especially missing short spacings), and probably higher closure errors in the older data. The closure errors are violations of the assumption made in self-calibration that all calibration errors are station dependent, affecting all baselines to a station equally. The ridge of low level signal to the south of

the core in 1982.77 and the various peaks surrounding the core in 1989.85 are artifacts resulting from closure errors. Also, from the experience gained while making the 1989.85 image, there appeared to be some uniqueness problems in the region of the jet between about 20 and 75 mas, so subtle details in that area should not be taken too seriously.

Figure 6 clearly shows that the bulge at about 200 mas is moving away from the core. The exact motion is hard to determine because the feature is large, without well defined compact components identifiable over the whole time. But estimates based on the outer edge, the southernmost extension, and an eyeballed estimate of the centroid, all constrain the total motion to be between 20 and 32 mas for a rate of 1.7 ± 0.4 mas yr $^{-1}$, or 3.5 ± 0.8 c for our assumed H_0 .

Figure 7 shows the central regions of the same images shown in Figure 6. For this figure, the vertical spacing between the images is proportional to the time separation between the observations. This explains why the 1982.77 and 1984.26 images have been cropped to allow them to be placed close together. With this vertical placement, any feature moving at constant velocity primarily in the horizontal direction will move along a straight line whose slope gives the speed. The alignment of the images along the jet direction has been done by aligning the image peaks. This is a reasonable choice, although if the peak feature is resolved, there may be a small shift from the optimum position. This may be a concern for 1984.85 and 1997.70. Any such offset should be less than about 2 mas.

In Figure 7, dark vertical lines have been drawn at the presumed core position and at the position of an apparently stationary feature that will be discussed below. Light shaded lines have been drawn to highlight what appear to be moving features. These lines are hand drawn suggestions of how to link up features. Clearly the structure of these images would not lend itself well to the Gaussian fitting procedures used at 5 GHz, especially in the regions more distant from the core. The same would probably be true at 5 GHz with similar quality images that showed the structure at larger core distances. An additional difficulty is that the sampling interval was sufficiently long during the 1984 to 1994 period to make association of features a bit problematic. Therefore the exact evolution of features cannot be precisely specified. But the lines are reasonable suggestions. All have slopes indicating feature speeds of between 2.5 and 3.1 mas yr $^{-1}$ (5.1 and 6.3 c) with uncertainties of about 10%. These speeds are similar to those of the faster 5 GHz features. Given the complexity of the structures and the difficulty of identifying exactly how to track features, these speeds are all the same to within the errors.

Note that two of the suggested features appear to pass through the stationary feature at 81 mas, brightening and moving to the south side of the jet in the process. Also note that the ridge line of the jet follows something of a twisted path that varies less between epochs than do the individual features. In particular, the bright region is along the northern side of the jet in the 60-70 mas region and farther out between 100 and 150 mas. The stationary feature at about 81 mas is brightest toward the southern side of the jet. These sorts of structures will be discussed below in terms of a possible helical path.

3. Discussion

The images presented in this study, along with the higher resolution, high frequency images of Gómez et al. (1998), Gómez, Marscher, & Alberdi (1999), and Gómez et al. (2000) make it clear that the 3C 120 jet is a continuous structure with brightness fluctuations that move down the jet at apparent superluminal speeds. The fact that the jet is a continuous structure is especially clear in the later (better) 1.7 GHz images which have a fairly smooth outer envelope despite strong fluctuations of brightness along the jet. Identifiable features in the brightness fluctuations can be followed for long distances as they move along the jet. Feature B was followed at 5 GHz from 1 to 15 mas over 5 years. Feature L7, seen at 1.7 GHz is likely to be a blending of several of the 5 GHz features including B and D and it is tracked to 50 mas from the core. Thus, whatever the brightness fluctuations are, they persist over large fractional core distances, suggesting that they mark a change in some fairly important jet parameter. A likely possibility is that they reflect changes in the amount of material moving down the jet. The enhanced brightness could be simply the result of increased density of emitting material. But it is also possible that a density change sets up conditions for shocks, which might be what is actually observed.

The big bulge seen moving down the jet between 200 and 250 mas at 1.7 GHz may represent an extreme case of a density enhancement. This feature appears almost like a lobe. It is seen best in Figure 5 where it clearly has a well defined outer edge and it has clearly pushed out the envelope of the jet to the south. This is reminiscent of the 15 mas scale jet in 3C 84 (Walker, Romney, & Benson 1994, and references therein) where a similar lobe-like structure can be traced back to a large flux density increase in about 1959. In both cases, the “lobe” is penetrating into a preexisting jet structure. The changes in jet characteristics are sufficiently pronounced that the appearance winds up similar to a large scale lobe interacting with an external medium. Note that the lobe speed of 1.7 mas yr^{-1} is somewhat less than the speeds of most of the components measured on smaller scales. This situation is also seen in 3C 84, although that source is not superluminal. This is consistent with the “lobe” structure being a region where material is piling up as it interacts with other, perhaps slower, material in the older jet. If this feature does represent a period of past increased activity, that occurred roughly 100 years ago.

The 5 GHz observations suggest that new superluminal components are emitted from the core of 3C 120 at intervals of under a year. In fact, this interval is mainly determined by a combination of the speed of the jet components and the angular resolution of the observations. At the observed angular rates of motion, features separated by significantly less than a year would not be resolved into separate components in our data. The higher resolution observations of Gómez et al. (1998) clearly show that there is complex structure on scales below our resolution. The birth of the brighter 5 GHz features is indicated by a brightening of the core at around the time of zero separation. This is likely also true for the weaker features, but the effect is disguised in the general variability of the core. After an initial brightening as they leave the core, the 5 GHz features decrease in brightness as they move down the jet. That decrease is monotonic in these data. The main exceptions seen in Figure 4 are the result of what is likely to be the poor amplitude calibration in 1983.25 noted

earlier. However note that the 1.7 GHz data presented here and the high frequency data of Gómez et al. (2000) show that a monotonic flux decrease is not a general property of components in the source.

The core is often, but by no means always, the brightest feature in the source. Some of the brightest moving features remain brighter than the core for up to about a year. For this reason, any attempt to do accurate geometric work such as geodesy or astrometry with this source must take structure into account in order to obtain results accurate to better than about 3 mas.

The speeds of features measured from the images presented here suggest that there is some variation in speed between components, but that variation is under a factor of two. At 5 GHz, speeds of between 1.5 and 3.5 mas yr⁻¹ are measured, but that range shrinks to 2.2 to 3.2 if only features seen in more than 3 images are included. The measured speeds are based partly on the assumption that the brightness fluctuations can be modeled as Gaussian components. That is clearly simplistic, and much blending of structures is involved. While the possibility that all features have the same speed is strongly excluded by the formal errors of the fits, it is not absolutely excluded when the reliability of the images and the difficulty of identifying some of the features at larger core distances are taken into consideration. However, note that Feature C, which is formally slower than Feature D, seems to disappear when Feature D catches up, supporting the idea that the speeds really do vary. Also the comparatively low speed of Feature J is reasonably convincing. In the 1.7 GHz images, all of the moving features less than 180 mas from the core have speeds similar to those of the 5 GHz features and to the speeds seen at 22 GHz close to the core in the movie of Gómez et al. (2000). There is a significant change at the 200 mas bulge, discussed above, which is clearly moving more slowly than features closer to the core. There is no clear evidence at either 1.7 or 5 GHz for a change of speed of an individual component.

The 3C 120 jet undergoes a significant bend on small scales. The high resolution images of Gómez et al. (1998) and Gómez, Marscher, & Alberdi (1999) show that it is first seen at submilliarcsecond scales to have a position angle of about -120° . Our 1.7 GHz images show an angle of roughly -100° out to about half an arcsecond. The high resolution images suggest that most of the curvature between these values occurs between about 2 and 5 mas. However our 5 and 1.7 GHz observations suggest that a position angle of near -105° is maintained as far as about 30 mas, at least in the more recent data. Some of the apparent curvature between 2 and 5 mas may be the result of internal side-to-side structure such as those at larger scales discussed below. Higher dynamic range, high resolution observations will clarify this.

It would be interesting to know how constant the position angle has been, especially on the small scales near the core. But unfortunately the very poor north-south resolution of the 5 GHz images makes it difficult to obtain accurate position angle measurements. The images of Figures 1, 2, and 3 do show that the position angle did not change much between 1979 and 1988. All images show position angles between the main features of between about -102 and -108° . A 1999 image at 5 GHz, currently being processed (Benson, private communication), and the high frequency

observations cited above, show a similar position angle except on scales of less than about 2 or 3 mas. On the smallest scales, the position angle is -120° or more negative. This could indicate that a real change in the position angle of the jet on the smallest scales has occurred. But it could simply show that the newer data, with improved north-south resolution, is better able to determine the position angle on these scales.

The evolution of components at 1.7 GHz is somewhat different from that seen at 5 GHz. The general decrease of brightness along the jet is apparent. But individual features can vary both up and down in brightness. In fact, there may be a pattern to where such variations occur, although the combination of the limited quality of the early epoch images and the poor time sampling make full delineation of such patterns problematic. The most probable case is the bright feature at about 81 mas that is there at some level in all 5 images. It appears that both features L4 and L5 pass through this feature. About 10 mas toward the core from this feature is a region that is relatively weak in all of the images. The bright feature is biased toward the southern side of the jet, while the weaker regions both closer to the core and farther out are to the north. This appears to be a stationary pattern superimposed on the moving jet. An eyeball estimate of the upper limit to the pattern speed is about 0.55 mas/yr or about $1.1c$, much slower than the speed of the knots. There are much less convincing hints of a similar pattern near 45 mas from the core. Such stationary patterns could result from a curved trajectory or from standing shocks, perhaps related to interaction with an external medium.

4. Implications of a Helical Pattern

The patterns described at the end of the last section are similar to those that would be expected if the brightest part of the jet followed a helical path on a cone. The brightest regions would be on the side where the path approaches closer to the line-of-sight. The brightness would be enhanced both by foreshortening, if the jet is optically thin, and by relativistic beaming, which increases at smaller line-of-sight angles. On the other side of the cone, the path would both be stretched out by projection and the brightness would be decreased because of reduced beaming. Figure 8, to be discussed in more detail later, shows the predicted appearance of a smooth jet following such a helical path. The region of the 3C 120 jet in the vicinity of the 81 mas (49 pc) feature looks much like the model, except that the jet is not smooth and components move along the path passing through the stationary pattern. The helix would be within the overall envelope of the jet since it is indicated by the line of brightest emission, not by the rather smooth outer limits to the jet sides.

Helical patterns are expected to occur in jets as the result of Kelvin-Helmholtz instability (Hardee 1987, 2000, and references therein), possibly driven by small perturbations near the central engine, so it would not be surprising to see a helical pattern in 3C 120. In this section we will discuss the implications of the observation of a helical pattern. But it should be kept in mind that the present data do not exclude other explanations for the structures seen. For example, shocks are often invoked in discussions of the nature of superluminal features and other brightness

fluctuations in jets. It is possible that the structures seen are the result of a combination of moving and stationary shocks. Monitoring at 1.7 GHz is continuing in an effort to improve the observational constraints.

Steffen et al. (1995) have explored the implications of the possible helical paths of superluminal components in 3C 345. They consider the the helical trajectories implied by 4 different cases of conserving 3 of 4 possible quantities; kinetic energy, angular momentum, linear momentum in the jet direction, and jet opening angle. The 3C 345 trajectories open out toward straight lines which are better matched by their Case 3 in which the unconserved quantity is linear momentum along the jet axis. However the 3C 120 morphology, which shows suggestions of multiple cycles of the helix, looks more like their Case 2, which allows the angular momentum to vary. They note that this case is equivalent to that of the hydrodynamic isothermal helical model of Hardee (1987).

The possible observation of a slowly moving, long wavelength, helical pattern has implications for the jet orientation and for the nature of the medium through which the jet propagates. To explore these implications, we first consider a simple morphological model which can be used to deduce some deprojected properties of the jet under the assumption that the helical pattern actually traces the path taken by jet material. We then consider how such a model relates to the flow through a helical pattern deduced from the time dependent linearized fluid equations. The theory suggests that an observed helical pattern may imply larger transverse motion than is experienced by individual fluid elements, thereby relaxing the constraints on the geometry. Finally we consider the implications of a slow pattern speed. A summary of the models considered and their implications is given in Table 5.

4.1. A Simple Model

For the simple model, we assume that the jet follows a helix that lies along the surface of a cone and has a wavelength that is a constant multiple of the cone radius, that the pattern is fixed, that the flow follows the pattern, and that the jet is optically thin. This corresponds to Case 2 of Steffen et al. (1995). The observed cone opening angle and helix wavelength constrain the true opening angle and wavelength as a function of the angle of the cone axis (hereafter called the jet axis) to the line-of-sight, θ . The observed superluminal motion constrains the jet speed in the direction of the jet axis, since it is an average speed. But the jet material has velocity components in other directions in order to follow the helix, so the required γ is somewhat higher than the usual $\gamma \approx \beta_{obs} = v_{obs}/c$ of a straight jet and is constrained by the geometry as a function of θ . With these constraints, the minimum and maximum angles to the line-of-sight of the flow along the pattern, and hence the beaming factors and projection effects, can be determined as a function of θ . The implied brightness difference between the brightest and dimmest parts of the pattern is a strong function of θ in this model and so can be compared with the images to constrain that angle.

To match 3C 120 with calculations of the sort described in the next paragraph, we used an

apparent (projected) half opening angle of the cone of 6° , a helix wavelength such that a full cycle occurs between the possible 45 mas feature and the 81 mas feature (27 and 49 pc at the assumed distance), an apparent average speed of 5.7 c, and a ratio of brightnesses of 20. We assumed a typical optically thin jet spectral index of $\alpha = -0.7$ ($S \propto \nu^\alpha$). A reasonable match to all of these constraints is given if the cone has an intrinsic half opening angle of 0.16° , is at 1.5° to the line-of-sight, has a helix wavelength of $\lambda = 120R$ (R is the jet radius) and has $\gamma = 9$. One fairly general property of a helix with the assumed projected wavelength and opening angle is that the path swings almost directly into the line-of-sight on one side.

Figure 8 shows the appearance of a simplified jet with the above properties. The “jet” consists of a continuous stream of unresolved, optically thin emitters following a fixed helical path on the surface of a cone at constant speed. The emitters are started along the jet at equal intervals and are of constant brightness in their rest frames. The position of each emitter, at the time the observed wavefront passes it, is calculated along with its beamed brightness. The crosses in the figure show the “observed” positions of the emitters on the plane of the sky. No attempt has been made to account for brightness evolution as the emitters move down the jet (dimming expected) or to model the brightness variations along the jet that are seen as components in the real data. The beamed flux density from each emitter is convolved with an observing beam, equivalent to that used for the 1.7 GHz images (with our assumed H_0), and added to the model image. The brightness enhancements where the jet swings into the line-of-sight on the southern side of the jet are obvious as are the dimmer looping structures along the northern side of the jet between the bright regions.

The modeled jet has a high degree of collimation with a pattern that only slightly deviates from longitudinal, but is both broadened and foreshortened by the projection effects of being very close to the line-of-sight. It is considerably closer to the line-of-sight than is required by the usual model for superluminal motion in a straight jet. In the straight jet model, $\gamma \approx \beta_{obs}$ and θ is assumed to be about $1/\gamma$, although a fairly wide range of angles is possible. For 3C 120, a straight jet would have $\gamma \approx 5.7$ and $\theta \approx 10^\circ$ with values up to near 20° possible. But for larger angles such as these, a helical jet matching the observed speeds and opening angle would have much too high a brightness contrast between the peaks and regions between the peaks.

There are at least two ways that the brightness contrast might be reduced, thus allowing higher angles to the line-of-sight and less severe collimation. It is possible that not all of the emitting material participates in the helical path, as is suggested by the relatively smooth outer jet boundary. Such emission could dominate between the peaks, reducing the observed brightness ratio. However in that case, it seems likely that the brightness would be distributed more evenly across the jet between the peaks, contrary to the observations. The other possibility is that the observed opening angle of the jet does not reflect the actual deviations of the material flow from the direction of the jet axis. The high pressure, and hence brightest, region may swing more widely than the actual particles as the jet flows through the helix. This would reduce the differential beaming effects and smooth the appearance of the jet. As noted below, physical models suggest that this will be the

case.

4.2. Physical Theory; Decoupling the Pattern and the Material Paths

Studies involving both physical theory and numerical simulation show that helical patterns are likely to form in jets, including relativistic jets. Hardee (1987, 2000) has shown that helical patterns are an expected result in many circumstances, can induce significant transverse motion without the development of shocks, and can produce asymmetries in Doppler boosted emission if jets are observed at line-of-sight angles on the order of the beaming angle. In particular, the theory has been compared to observations, especially of M 87, which shows helical patterns (Owen et al. 1989). But one difficulty is that the theoretical helical patterns, and those observed in M 87, are much more tightly wound than what we see in 3C 120. The fastest growing unstable modes in these calculations typically have wavelengths of only a few jet radii. These calculations generally assume a hot jet in a hot medium (like a cocoon). But the wavelength of the fastest growing structures increases if the jet sound speed is lower (higher internal Mach number) and/or the Lorentz factor is higher, provided that the ambient (external) sound speed is much less than the jet sound speed. This suggests that the 3C 120 jet resides in a relatively cool medium, and not in a relativistically hot cocoon or lobe.

The linearized time dependent fluid equations give the distribution of pressure and fluid velocity field within the jet as fluid moves through a helical pattern. Typically the highest pressures are near the surface of the jet at an azimuthal position that rotates with the phase of the pattern. The actual jet material need not follow the path of the region of highest pressure. In general the flow lines will follow a smaller diameter helical path than the region of highest pressure. The brightest radio emission is expected to be generated in the region of highest pressure so the observations will trace the path of that region. But one cannot use that path to calculate the relativistic beaming effects because they depend on the vector velocity of the emitting material. In principle, the reduced helical path followed by the material allows for lower brightness variations than are calculated assuming that the apparent path is the material path. A general result of calculations from the fluid equations is that, as one moves to shorter pattern wavelengths, the transverse motions become smaller so the suppression of beaming-induced brightness contrasts becomes larger.

We have modified the simple model described earlier to allow for material following tighter helices than the apparent path of the brightest emission. With this modified scenario, it is possible to find parameters that predict an appearance and apparent velocity that are very similar to the predictions of the model used above to fit the 3C 120 data, but with much wider angles between the average jet axis and the line-of-sight. A fit can be obtained with essentially any angle to the line-of-sight up to at least 16° . As that angle increases, the required ratio of the radius of the apparent helical path described by the brightest emission to the effective radius of the helical path followed by the material increases. For 10° to the line-of-sight, the apparent helical path must be about 2.2 times the effective radius of the helical path followed by the material. For 16° , the ratio

would be about 4.6.

As the angle of the jet to the line-of-sight increases, the helical wavelength required to approximate that seen in projection in the 3C 120 images decreases. To compare with the theory, we need to relate the helical wavelength to the jet radius, and it is no longer obvious how that radius relates to features in the images. But assuming that the path of brightest emission marks the edge of the jet, the wavelengths for the models at 10° and 16° to the line-of-sight have wavelengths of 33 and 21 times the radius. This is much shorter than that implied by the original model with its very small angle to the line-of-sight, but is still large compared to the situation analyzed for M87. Ultimately, this sort of analysis should be done by including the radio emission, along with beaming effects, in the physical theory or numerical models.

4.3. Moving Patterns

One difference between the simple morphological model and a helically twisted jet is that the helical pattern will be moving. Motion of a large scale helical pattern can be computed from the linearized time dependent fluid equations, e.g., Hardee (2000). While in general the pattern speed is a function of the wavelength, at very long wavelengths relative to the most Kelvin-Helmholtz unstable helical wavelength (see eq. [7b] in Hardee 2000), the pattern speed may be found from the real part of (eq. [5a] in Hardee 2000)

$$\omega/ku \approx \frac{\gamma^2 \eta_{rel}}{1 + \gamma^2 \eta_{rel}} \pm i \frac{\gamma \eta_{rel}^{1/2}}{1 + \gamma^2 \eta_{rel}}.$$

Here γ is the Lorentz factor of the underlying flow with speed u and $\eta_{rel} \equiv (a_{ex}/a_{jt})^2$, where a_{ex} and a_{jt} are the sound speeds external to and inside the jet respectively. The sound speed is $a \equiv [\Gamma P_0/(\rho_0 + [\Gamma/(\Gamma - 1)]P_0/c^2)]^{1/2}$, where $4/3 \leq \Gamma \leq 5/3$ is the adiabatic index. The density, ρ_0 and pressure, P_0 , are measured in the proper fluid frame, and since pressure balance has been assumed η_{rel} is effectively an enthalpy ratio. At the most unstable wavelength

$$\lambda \approx 3.75 \frac{\gamma [M_{jt}^2 - u^2/c^2]^{1/2} M_{ex}}{[M_{ex}^2 - u^2/c^2]^{1/2} + \gamma [M_{jt}^2 - u^2/c^2]^{1/2}} R,$$

the pattern speed is approximately given by (eq. [7c] in Hardee 2000)

$$v_w \approx \frac{\gamma [M_{jt}^2 - u^2/c^2]^{1/2}}{[M_{ex}^2 - u^2/c^2]^{1/2} + \gamma [M_{jt}^2 - u^2/c^2]^{1/2}} u,$$

where $M \equiv u/a$. In general, we expect that any large scale helical twist and observed helical pattern to have a pattern speed that lies between the values at long wavelength and at the most unstable wavelength. In the absence of a low frequency precession at the central engine, the most unstable wavelength is the one most likely to grow and be seen. Helical wavelengths shorter than the most unstable wavelength will not move the whole jet bodily but can still produce a helical

pattern near to the jet surface. In general, the shorter helical wavelengths propagate with much higher pattern speeds.

A long stationary pattern wavelength such as we assume for 3C 120 suggests that η_{rel} is small and that M_{ex} is large, as this sets an upper limit to any helical pattern speed to be significantly less than c . Because of projection effects, and a speed that is too low to amplify the apparent speed as for superluminal motion, such a pattern would appear to be stationary in our data, consistent with our results. Thus, a cool and not a relativistically hot external cocoon or lobe medium is implied for a long wavelength pattern that is relatively slowly moving. This is the same conclusion that was reached in section 4.2 from the desire to have the most unstable modes be of long wavelength to match the observations.

While the helical pattern is not moving superluminally, the apparent helical wavelength in the observer frame would be affected by any motion. The observed radiation travels nearly parallel to the jet so, in the time it takes to go between points where the pattern is at the same azimuth with respect to the jet axis, the pattern has moved. The apparent observed pattern is stretched as

$$\lambda^{obs} = \left(\frac{1}{1 - \beta_w \cos\theta} \right) \lambda$$

where $\beta_w = v_w/c$. For example, a helix with a wavelength of $80R$ in the pattern frame moving with a pattern speed $c/3$ at an angle of 3° to the line-of-sight has an observed wavelength of about $120R$. A second effect of a moving helix is that fluid does not need to move as rapidly in the transverse direction to circulate through the helix as the fluid does for a “stationary” helix. The two effects will modify the Doppler boosting somewhat, although the two effects will tend to cancel each other as the stationary helical path has a longer intrinsic wavelength than the moving helical path. To investigate these effects we have computed, from the linearized time dependent fluid equations, the velocity components of material moving through a $120R$ nearly stationary helix (pattern speed $c/100$) and for a $80R$ moving helix (pattern speed $c/3$), both with transverse helical displacement of the jet by $1/2$ the jet radius. There is very little difference in the transverse velocity components for the two cases. At least approximately (the flow angle is not exactly the same over the jet cross section), the flow angle with respect to the jet axis is about the same for the stationary helix and for the moving helices. Thus, we expect calculations for a stationary $120R$ helix to be only slightly modified if a helical pattern speed is considered. Similar effects would be expected for the shorter wavelengths allowed by the decoupling of the pattern and material paths. One goal of extended monitoring observations is to provide much improved constraints on the pattern speed.

Additional computations help constrain the angle of the jet to the line-of-sight. As noted earlier, the limited brightness contrasts along the pattern cannot be used to do this because transverse motions of the material may be considerably smaller than implied by the observed pattern. But the limits on the observed pattern speed can provide constraints. Larger line-of-sight angles require deprojected helical pattern wavelengths that are shorter than the fastest growing helical wavelength. While we cannot completely rule out shorter somewhat more rapidly moving helical patterns, preliminary computations suggest that the observed pattern wavelength must be longer

than the most unstable wavelength if the observed pattern speed is to appear stationary in the data. Given the pattern speed appropriate to the most unstable wavelength, we find that the shortest deprojected wavelength consistent with the measured upper limit to the pattern speed is given by

$$\lambda \approx 3.75 \frac{\gamma [M_{jt}^2 - u^2/c^2]^{1/2} M_{ex}}{[M_{ex}^2 - u^2/c^2]^{1/2}} R .$$

In the above expression we have assumed that $\cos\theta \approx 1$ and that $(1 - u/c) \ll 1$. Models involving line-of-sight angles larger than about 10° require a deprojected observed helical wavelength shorter than this limit and thus would show too high a pattern speed. Note that these arguments imply that the tightly wound helix seen in M87 would have a high pattern speed.

4.4. Helical and Other Patterns Elsewhere in 3C 120

Patterns reminiscent of a helix are seen on other scales in 3C 120. On scales between about 1 and 15 arcseconds, there are several cycles of an oscillating pattern that could be a helix (Walker 1997), again with a long wavelength. In fact the $4''$ knot, whose motions were the object of study of Walker (1997), could, from morphological grounds, be another feature like the one at 81 mas. This reinforces the idea, mentioned in the introduction, that the lack of motion in this feature does not indicate that the jet material has slowed. Gómez et al. (1998) suggest that the structures observed at 22 and 43 GHz in 3C 120 at about 3 to 5 mas from the core are the result of a helical path on a much smaller scale than what we see at 1.7 GHz. As with our results, the wavelength is long, even in projection, relative to the jet radius. But, more extensive monitoring has suggested another explanation related to interaction with a cloud intermediate in mass between narrow and broad line clouds (Gómez et al. 2000). This provides a cautionary note against over interpreting the current data and shows the need for continued monitoring to clarify the situation.

The 3C 120 jet shows a number of pronounced curves that are probably not part of a helical pattern. The first is in the region of a few mas where the jet bends from a position angle of about -120° (Gómez et al. 1998) to the approximately -100° seen out to a few arcseconds. At about 6 arcseconds, the jet begins a long gentle curve that eventually takes it through an angle of at least 120° over several arcminutes on the sky before the structure becomes difficult to interpret (Walker, Benson, & Unwin 1987; Walker 1997). These curves are probably real bends in the jet. Because of projection at the small angle to the line-of-sight, such curves need only be through a few degrees. They may be the result of interaction with an external medium as suggested by the pronounced side-to-side asymmetry between 5 and 25 arcseconds seen in the image in Walker (1997).

5. Conclusions

The main conclusions of this study are:

- The 3C 120 jet is a continuous structure with brightness variations. Identifiable features in the brightness structure move down the jet at superluminal speeds. We are able to identify new features appearing at intervals of less than a year (Figure 4, Table 4), an interval that is set mainly by a combination of the jet speed and the angular resolution of the observations. Finer scale structure is known to exist as shown by higher frequency observations by other groups (c.f. Gómez et al. 2000)
- The two best 1.7 GHz images show structure with large variations of brightness along the jet, but a fairly smooth outer envelope of the emitting region (Figure 5).
- The speeds of the 5 GHz components in the region between 1 and 10 mas of the core appear to vary over a range that is well under a factor of two (Table 4). The formal errors strongly exclude the possibility that the speeds are all the same. But because of the limited image reliability and the difficulty in identifying some of the features at larger core distances, that conclusion is not as firm as the formal statistics would suggest.
- On the larger scales sampled by the 1.7 GHz images, most of the moving features have angular rates in the 2.5 to 3.1 mas yr^{-1} range, and within the uncertainties, could all be the same (Figure 7). This is within the range of speeds seen at higher resolution in our 5 GHz observations and in the 22 and 43 GHz observations of Gómez et al. (1998). The fact that the speeds show the same fairly narrow range between a few tenths of a parsec to about 120 parsecs in projection indicates that there are not large changes in either the underlying speed or angle to the line-of-sight of the jet in that range. The observed superluminal motions place an upper limit on the angle to the line-of-sight of about 20° so the 120 pc deprojects to at least 350 pc with much larger values more likely.
- The outermost feature for which a speed could be determined is the bulge at around 200 mas (Figure 6). It is moving at a rate of 1.7 mas yr^{-1} , which is slower than most of the features closer to the core, especially those with reliable speed measurements. This may be the leading edge of material ejected during a period of enhanced activity. It is now plowing into the older jet material plus expanding the jet, a situation similar to that seen in 3C 84 (Walker, Romney, & Benson 1994). Such features in radio sources may constitute a fossil record of previous periods of enhanced activity, about 100 years ago in this case.
- The 1.7 GHz data show evidence that there are both moving and stationary features in the same regions (Figure 7). In fact, it appears that moving components can pass through a stationary feature, dimming or brightening as they do so. The stationary features could either be places of interaction with the external medium or could reflect changes in jet direction with corresponding changes in the intensity of the relativistic beaming.
- The stationary brightening regions have structure reminiscent of the feature at $4''$ which also appears to be stationary to within the measurement errors (Walker 1997). This enhances the suspicion that the $4''$ knot's lack of motion does not imply that the underlying jet is not

relativistic. The knot may, like the stationary brightening regions in the 1.7 GHz images here, be regions of interaction with the external medium or a result of jet bending, perhaps as part of a helical pattern. The lack of a visible counterjet, despite the presence of a counter lobe on scales of several arcminutes, is further evidence that the jet remains relativistic to large scales.

- Some of the features seen in the 1.7 GHz images suggest that the jet has a helical structure. To match the observed structure, either the jet must be extremely close to the line-of-sight (much closer than the maximum angle allowed by the superluminal motion alone) or there must be an offset between the line traced by the peak brightness and the path of individual fluid elements. The fluid equations (e.g., Hardee 2000) applied to helically twisted jets predict such an offset because the region of high pressure describes a helix of larger transverse amplitude than is followed by the fluid elements. Additional theoretical constraints related to the low pattern speed suggest that the jet is closer to the line-of-sight than about 10° . For any line-of-sight angle allowed by the superluminal motion, the wavelength of the helix is relatively long, in contrast to the situation in M87 where tightly wound helical patterns are seen. Longer wavelengths are favored when the jet is surrounded by a relatively cool medium.

The picture that emerges is one of a continuous, relativistic jet with much internal structure but a smooth outer envelope. The velocity is maintained from sub-parsec to hundreds of parsec scales. There is some slowing at the largest scale feature whose speed could be measured, but the jet appears to remain relativistic to kiloparsec and larger scales. The structure includes both features that move with the jet, perhaps density enhancements or shocks, and also features that do not move with the flow. The moving features can pass through the stationary features, suggesting that the stationary features do not significantly disrupt the flow. These could be places where there is some interaction with the external medium or they could be the result of variations in the jet path. Individual features are followed for large fractional distances from the core, suggesting that they represent variations in fundamental and enduring parameters of the jet such as density. Possible helical patterns of long wavelength are seen on several scales. Theoretical arguments suggest such wavelengths when the jet is cool and/or of high Lorentz factor and is moving through a cool and not relativistically hot medium.

We would like to thank the staffs of all the observatories listed in the Table 1 and the Caltech, Charlottesville, and Socorro correlators, without whose efforts these observations would not have been possible. While we did not use their data directly in the above text, we often consulted the University of Michigan Radio Astronomy Observatory flux density history available on the Internet for a consistent history of activity in 3C 120. That project is supported by funds from the University of Michigan. T. Hunter and M. Lystrup acknowledge support as summer students at NRAO by the Research Experiences for Undergraduates program of the National Science Foundation. P. Hardee acknowledges support from the National Science Foundation through grant AST-9802955 to the

University of Alabama. P. Hardee and C. Walker acknowledge the Aspen Center for Physics where some of this work was performed.

REFERENCES

Axon, D. J., Unger, S. W., Pedlar, A., Meurs, E. J. A., Whittle, D. M., & Ward, M. J. 1989, *Nature*, 341, 631

Baldwin, J. A., Carswell, R. F., Wampler, E. J., Smith, H. E., Burbidge, E. M., & Boksenberg, A. 1980, *ApJ*, 236, 388

Benson, J.M., Walker, R.C., Unwin, S.C., Muxlow, T.W.B, Wilkinson, P.N., Booth, R.S., Pilbratt, G., & Simon, R. S. 1988, *ApJ*, 334, 560

Blandford, R. D. & Königl, A. 1979, *ApJ*, 232, 34

Briggs, D. 1995, Ph. D. thesis, New Mexico Inst. of Mining and Technology

Burbidge, E. M. 1967, *ApJ*, 149, L51

Clark, B. G. 1973, *Proc. I.E.E.E.* 61, 1242

Gómez, J. L., Martí, J. M., Marscher, A. P., Ibáñez, J. M., & Alberdi, A. 1997, *ApJ*, 482, L33

Gómez, J. L., Marscher, A. P., Alberdi, A., Martí, J. M., & Ibáñez, J. M. 1998, *ApJ*, 499, 221

Gómez, J. L., Marscher, A. P., & Alberdi, A. 1999, *ApJ*, 521, L29

Gómez, J. L., Marscher, A. P., Alberdi, A., Jorstad, S. G., & Garcia-Miró, C. 2000, *Science*, 289, 2317

Grandi, P, Sambruna, R. M., Maraschi, L., Matt, G., Urry, C. M., & Mushotzky, R. F. 1997 *ApJ*, 487, 636

Halpern, J. P. 1985, *ApJ*, 290, 130

Hardee, P. E. 1987, *ApJ*, 318, 78

Hardee, P. E. 2000, *ApJ*, 533, 176

Harris, D. E., Hjorth, J., Sadun, A. C., Silverman, J. D., & Vestergaard, M. 1999, *ApJ*, 518, 213

Hjorth, J., Vestergaard, M., Sørensen, A. N., & Grundahl, F. 1995, *ApJ*, 452, L17

Homan, D. C. & Wardle, J. F. C. 1999, *AJ*, 118, 1942

Hua, C. T. 1988, *A&A*, 199, 105

Lyutyi, V. M. 1979, Soviet Astr., 23, 518

Maraschi, L., Chiapetti, L., Falomo, R., Garilli, B., Malkan, M., Tagliaferri, G., Tanzi, E. G., & Treves, A. 1991, ApJ, 368, 138

Moles, M., del Olmo, A., Masegosa, J., & Perea, J. D. 1988, A&A, 197, 1

Muxlow, T. W. B., & Wilkinson, P. N. 1991, MNRAS, 251, 54

Napier, P. J., Bagri, D. S., Clark, B. G., Rogers, A. E. E., Romney, J. D., Thompson, A. R., & Walker, R. C. 1994, Proc. IEEE, 82, 658

Oke, J.B., Readhead, A. C. S., & Sargent, W. L. W. 1980, PASP, 92, 758

Owen, F. N., Hardee, P. E., & Cornwell, T. J. 1989, ApJ, 340, 698

Peterson, B. M., Wanders, I., Bertram, R., Hunley, J. F., Pogge, R. W., & Wagner, R. M. 1998, ApJ, 501, 82

Pollock, J. T., Pica, A. J., Smith, A. G., Leacock, R. J., Edwards, P. L., & Scott, R. L. 1979, AJ, 84, 1658

Seielstad, G. A., Cohen, M. H., Linfield, R. P., Moffet, A. T., Romney, J. D., Schilizzi, R. T., & Shaffer, D. B. 1979, ApJ, 229, 53

Steffen, W., Zensus, J. A., Krichbaum, T. P., Witzel, A., & Qian, S. J. 1995, A&A, 302, 335

Walker, R. C., Seielstad, G. A., Simon, R. S., Unwin, S. C., Cohen, M. H., Pearson, T. J., & Linfield, R.P. 1982, ApJ, 257, 56

Walker, R. C., Benson, J. B., & Unwin, S. C. 1987, ApJ, 316, 546

Walker, R. C., Romney, J. D., & Benson, J. M. 1994, ApJ, 430, L45

Walker, R. C. 1997, ApJ, 488, 675

Wandel, A., Peterson, B. M., and Malkan, M. A 1999, ApJ, 526, 579

Wlerick, G., Westerlund, B., & Garnier, R. 1979, A&A, 72, 277

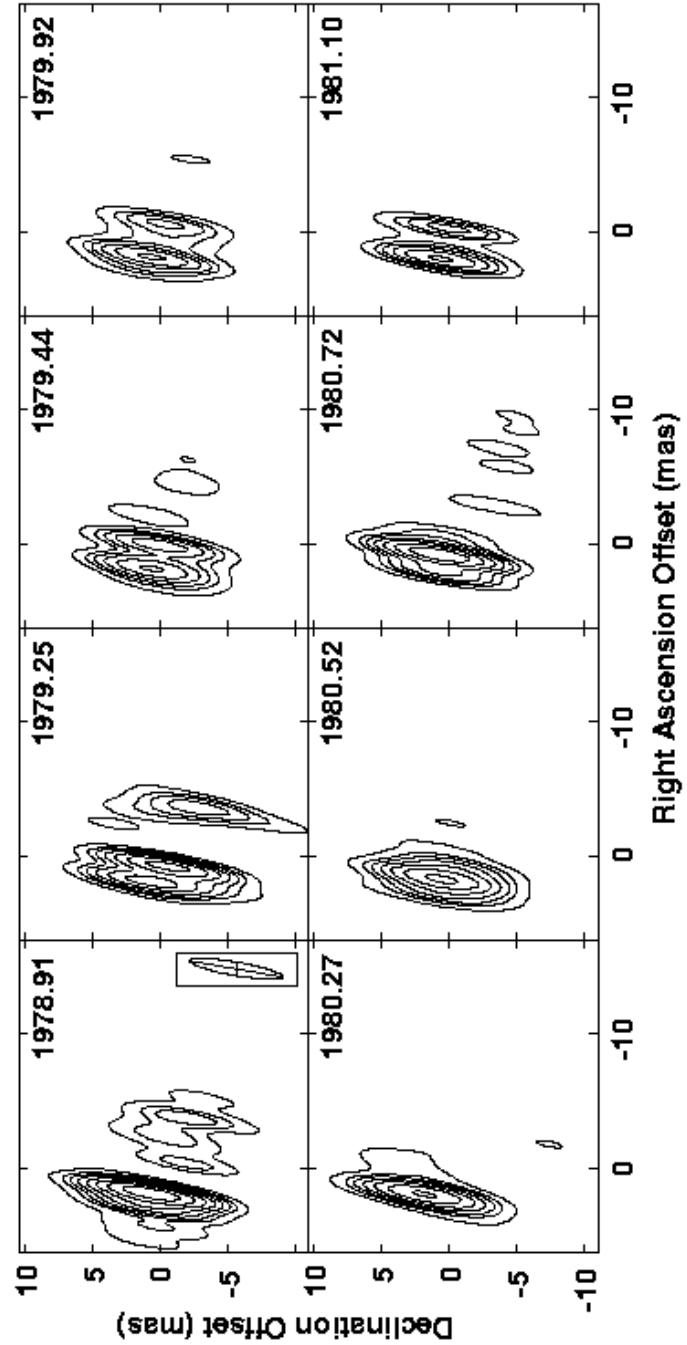


Fig. 1.— The images from the 3C 120 Network VLBI monitoring program between 1978.91 and 1981.10. The images were made at either 5 or 10.7 GHz; see Table 2 for details. All are images made from CLEAN components convolved with a elliptical Gaussian beam 7.0 by 1.0 mas, elongated along position angle -10° . The contour levels are 0.1, 0.2, 0.28, 0.4, 0.57, 0.8, 1.13, and 1.60 Jy beam $^{-1}$. The peak flux densities are tabulated in Table 2.

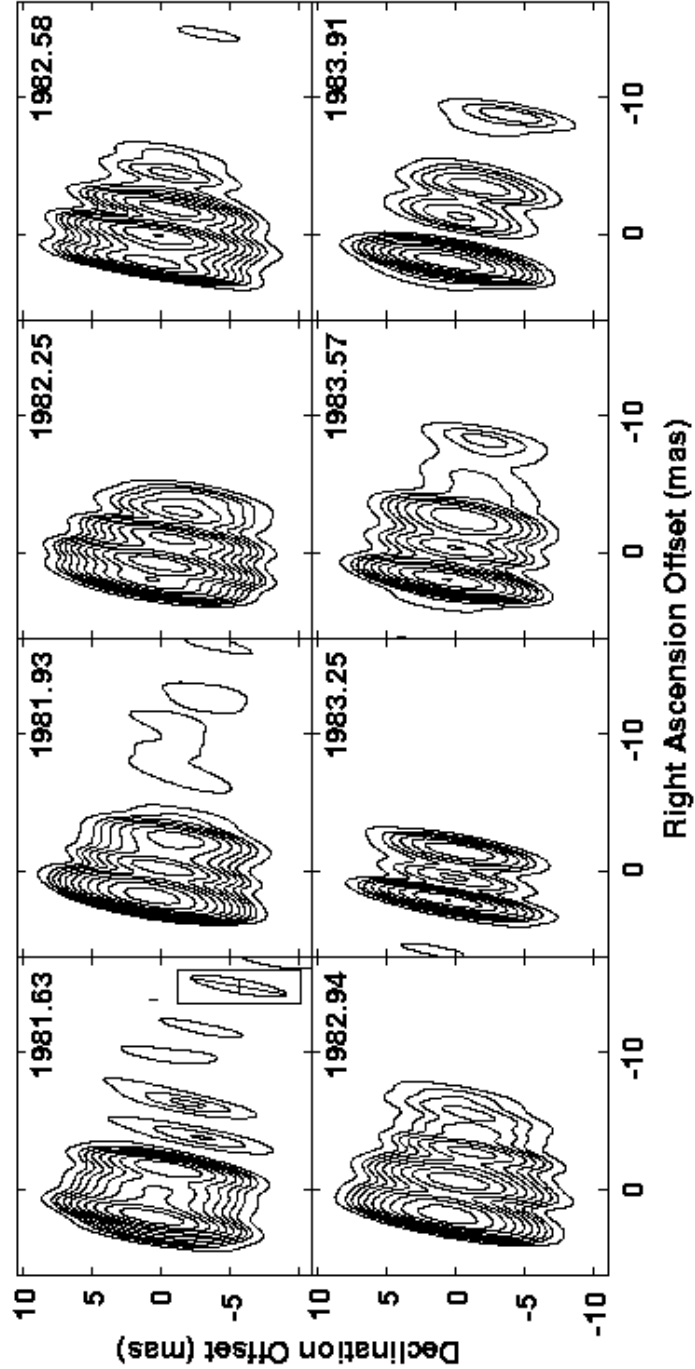


Fig. 2.— The images from the 3C 120 Network VLBI monitoring program between 1981.63 and 1983.91. The images were made at 5 GHz. All are images made from CLEAN components convolved with a elliptical Gaussian beam 7.0 by 1.0 mas, elongated along position angle -10° . The contour levels are 20, 40, 57, 80, 113, 160, 226, 320, 453, 640, and 905 mJy beam $^{-1}$. The peak flux densities are tabulated in Table 2.

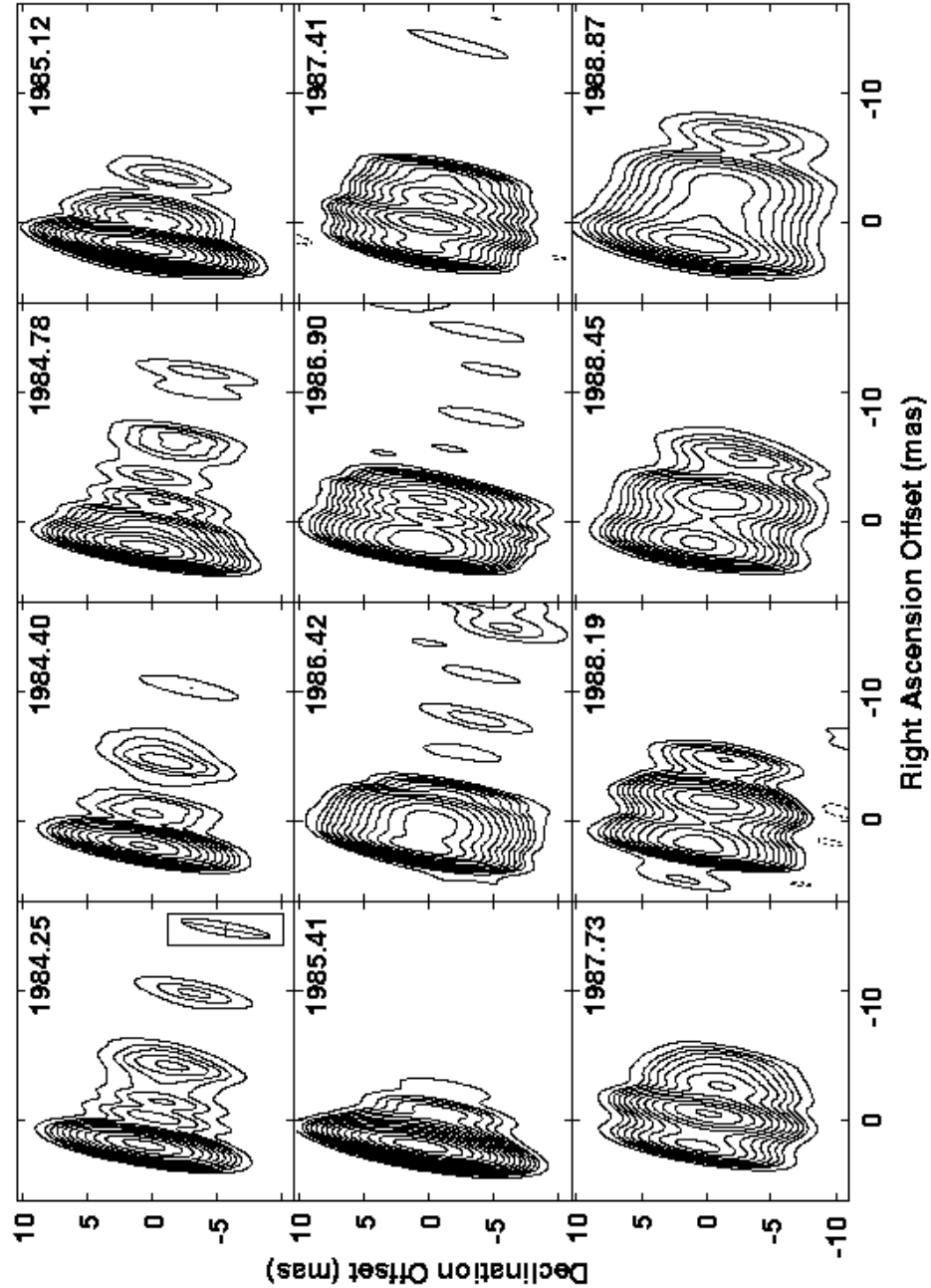


Fig. 3.— The images from the 3C 120 Network VLBI monitoring program between 1984.25 and 1988.87. The images were made at 5 GHz. The contour levels are $-10, 10, 20, 28, 40, 57, 80, 113, 160, 226, 320, 453, 640, 905, 1280$, and $1810 \text{ mJy beam}^{-1}$. The peak flux densities are tabulated in Table 2. All of the images are made from CLEAN components convolved with a elliptical Gaussian beam 7.0 by 1.0 mas, elongated along position angle -10° . Half have the CLEAN residuals restored to the image (1984.78, 1986.42, 1987.41, 1987.73, 1988.45, and 1988.87), but with the deep CLEANs used, this does not make much difference. The average off-source noise level in the images with residuals is $1.3 \text{ mJy beam}^{-1}$. That noise is dominated by calibration artifacts.

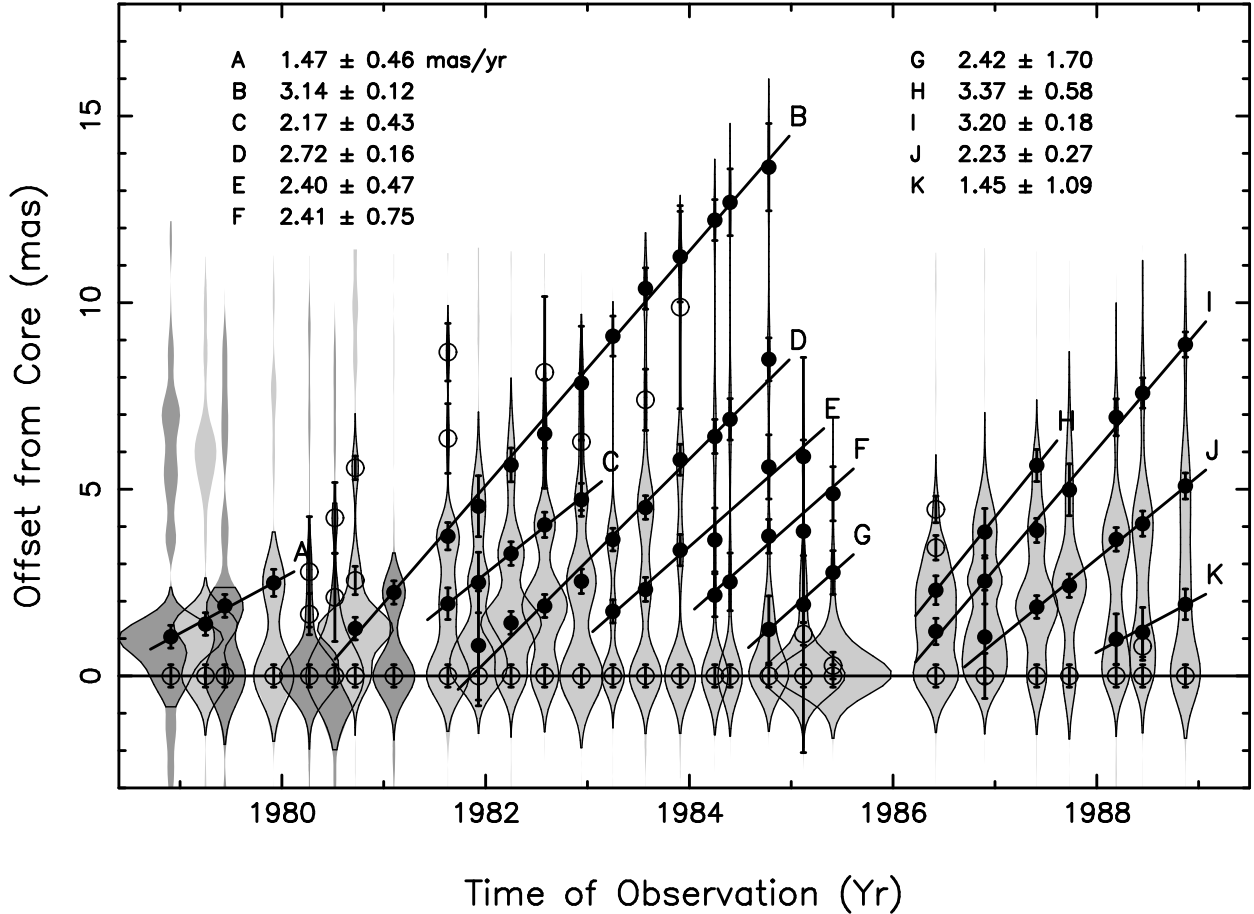


Fig. 4.— This figure shows the motions of components seen at 5 and 10.7 GHz in 3C 120 between 1978 and 1988. For each image, there is a shaded profile whose width represents the amplitude along a slice that runs along the ridge line of the jet. The 10.7 GHz images are indicated by darker shading. The thin lines that appear to outline the shading are the results of Gaussian fits to the reliable parts of the slices. The profiles have been aligned on the eastern-most feature, presumed to be the core. The fitted positions, relative to the core, of other features are shown by circles with error bars that reflect the combined formal position errors for that feature and for the core, along with an assumed alignment error. Features with filled circles are ones that are identifiable at multiple epochs and for which speeds are measured with a least squares fit. The components are labeled and a straight line with the slope corresponding to the fitted velocity is drawn through the points. The velocity for each feature, with formal errors, is written on the figure and listed in Table 4.

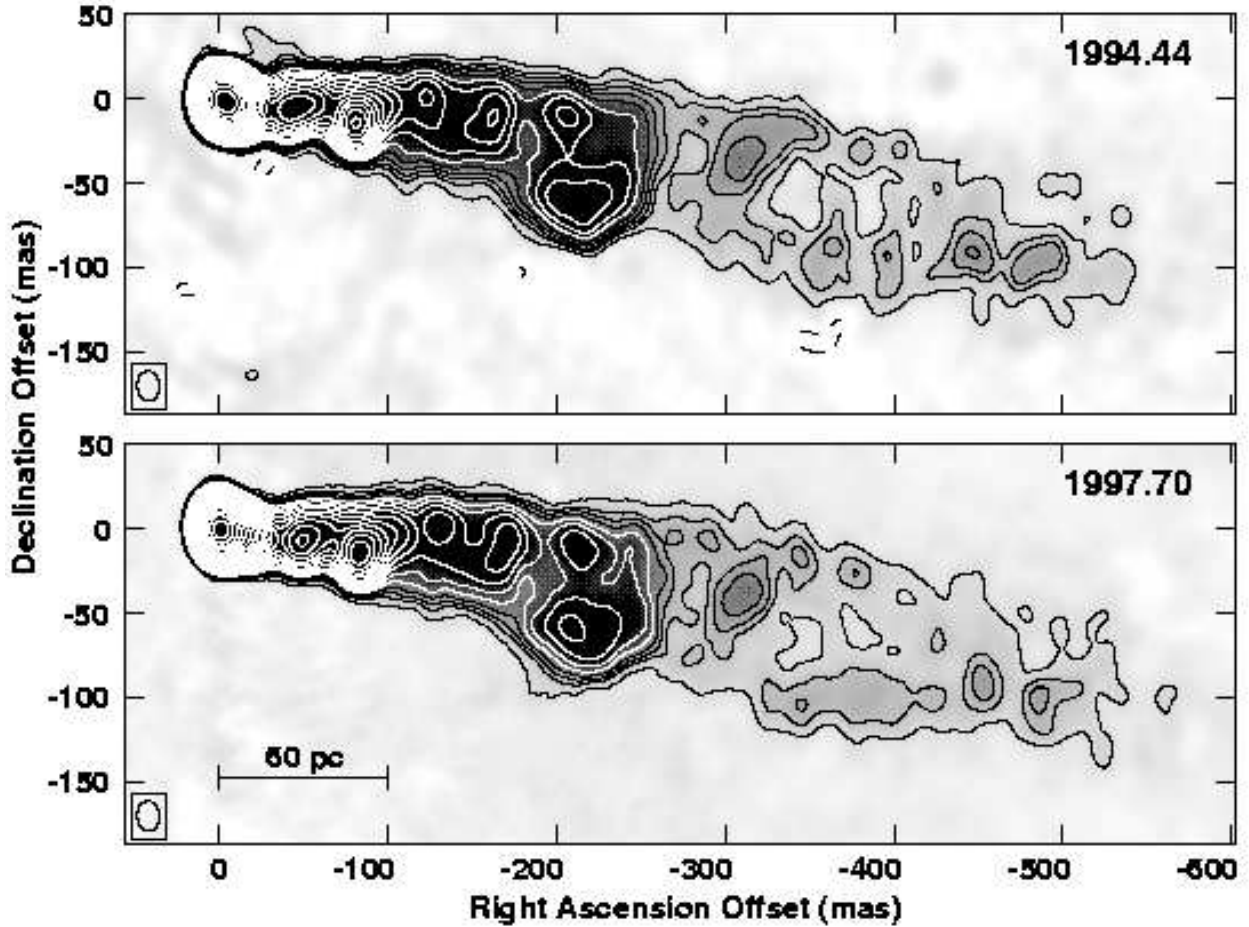


Fig. 5.— Low resolution versions of the 1.7 GHz images from 1994.44 and 1997.70. These were the epochs that used wide band recording systems and had the sensitivity to see the structures between 270 and 540 mas from the core. Both of these images have been made with a taper that uses mainly the continental and shorter baselines. They were convolved with a common beam of 18 by 13 mas at position angle 3° . The contour levels are $-1.4, -1.0, -0.5, 0.5, 1.0, 1.4, 2.0, 2.8, 4.0$ mJy beam $^{-1}$ with the higher levels increasing by factors of $\sqrt{2}$ from there. The image peaks are 1.42 and 1.83 Jy beam $^{-1}$ in 1994.44 and 1997.70 respectively. The off-source rms noise levels are 0.15 and 0.10 mJy beam $^{-1}$. The scale bar is based on $H_0 = 75$ km s $^{-1}$ Mpc $^{-1}$.

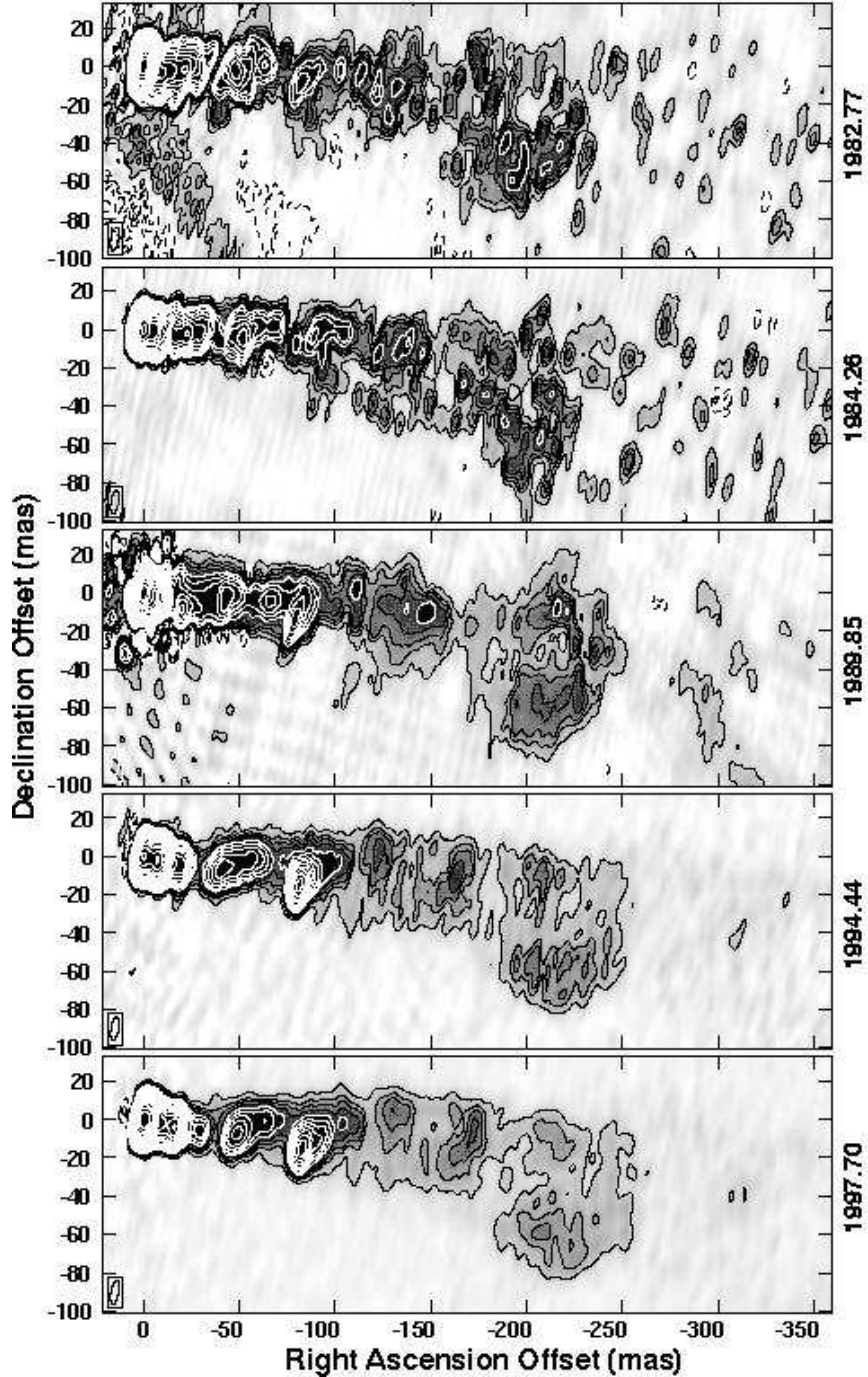


Fig. 6.— The inner 360 mas of the 5 images available at 1.7 GHz. All have been convolved to a common beam of 12.5 by 4.0 mas elongated in position angle -10° . The lower contour levels are $-2.1, -1.5, -0.75, 0.75, 1.5, 2.1, 3.0, 4.2, 6.0$ mJy beam $^{-1}$ with the higher levels increasing by factors of $\sqrt{2}$ from there. The peak flux densities and noise levels can be found in Table 3.

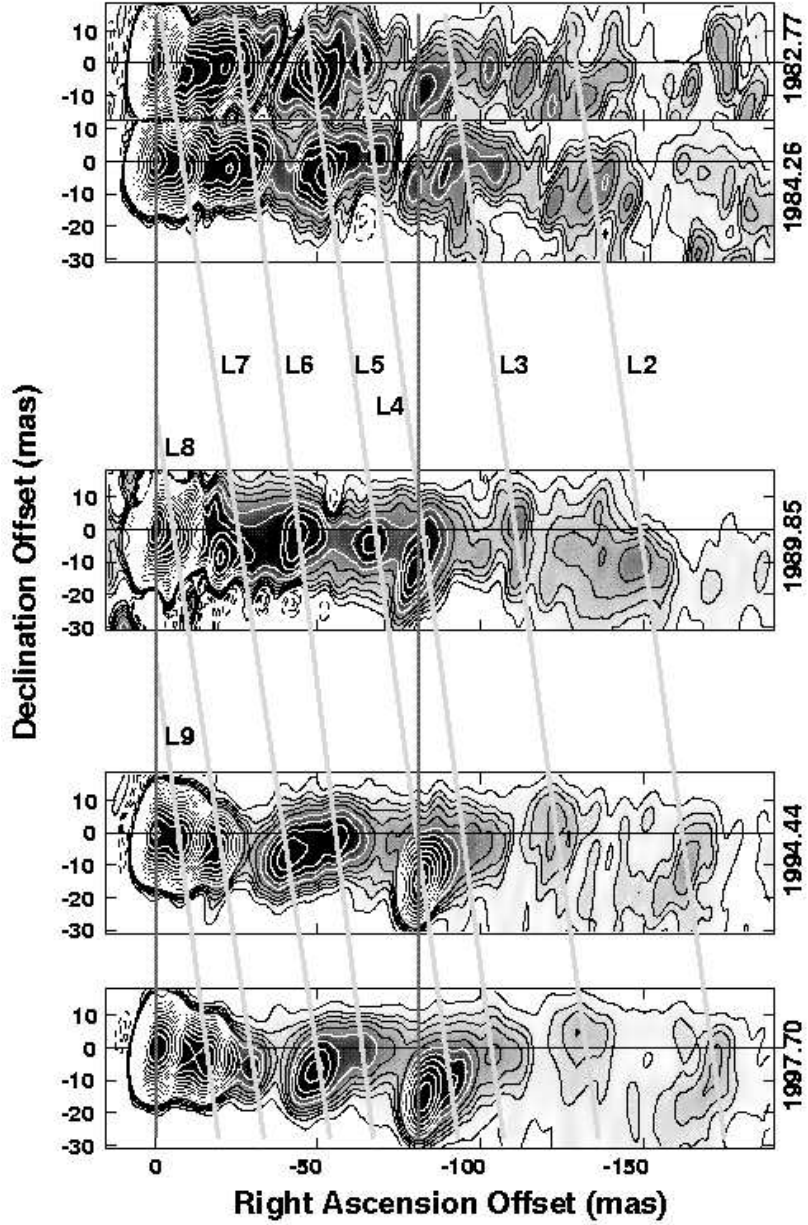


Fig. 7.— The inner 190 mas of the 5 images available at 1.7 GHz. These are the same images with the same contour levels as those in Figure 6. The images have been spaced vertically on the page so that the separations between the cores is proportional to the time intervals between the observations. This allows features moving with constant apparent speed to be marked with straight lines. The source appears to contain both moving and stationary features. A stationary feature and the core have been marked with dark vertical lines. The light lines are eyeball connections of moving features. All have slopes of between 2.5 and 3.1 mas yr⁻¹.

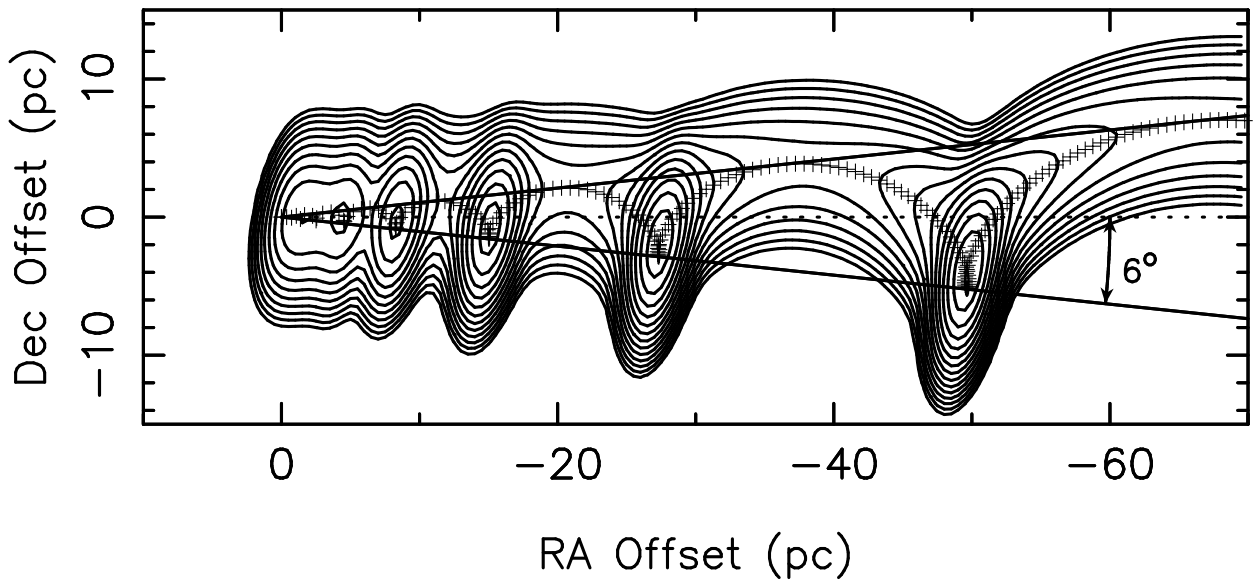


Fig. 8.— A contour image, with $\sqrt{2}$ levels, of the predicted structure of a simple helical jet. The crosses mark the sky-plane positions of test emitters at the time that the observed wave-front passed them. The test emitters follow a fixed helical path on the surface of a cone and are of constant brightness in their rest frames. The emission from the model points has been convolved with the 12.5 by 4.0 mas beam used in the 1.7 GHz images, scaled by 0.6 pc mas^{-1} . The solid lines outline the cone while the dotted line indicates the cone axis. The model is the one described in the text without any offset between the brightness ridge and the path of the particles. Other models with the particles following narrower spirals at higher angles to the line-of-sight, but with the brightest emission shifted toward the outside of the jet, produce very similar looking images.

Table 1. VLBI Antennas

Name	Code	Location	Diameter (m)
US VLBI Network:			
Arecibo	A	Puerto Rico	300
Haystack	K	Massachusetts	37
Green Bank 140'	G	West Virginia	43
North Liberty	I	Iowa	18
Fort Davis (GRAS)	F	Texas	26
VLA (single antenna)	Y1	New Mexico	25
VLA (phased array)	Yp	New Mexico	27 × 25
Owens Valley	O	California	40
Hat Creek	H	California	26
Maryland Point (NRL)	N	Maryland	26
European VLBI Network:			
Jodrell Mark I	J	United Kingdom	76
Jodrell Mark II	J2	United Kingdom	38 by 25
Onsala	S	Sweden	26
Westerbork (1 or 12 antennas)	W	The Netherlands	(12×) 25
Effelsberg	B	Germany	100
Medicina	M	Italy	32
Torun 18	T	Poland	18
Torun 32	Tr	Poland	32
Simeiz	R	Ukraine	22
Noto	Nt	Italy	32
VLBA:			
Saint Croix	Sc	Virgin Islands	25
Hancock	Hn	New Hampshire	25
North Liberty	Nl	Iowa	25
Fort Davis	Fd	Texas	25
Los Alamos	La	New Mexico	25
Pie Town	Pt	New Mexico	25
Kitt Peak	Kp	Arizona	25
Owens Valley	Ov	California	25
Brewster	Br	Washington	25

Table 1—Continued

Name	Code	Location	Diameter (m)
Mauna Kea	Mk	Hawaii	25
Other:			
Defford	U	United Kingdom	25
Cambridge	E	United Kingdom	18
Dwingeloo	D	The Netherlands	25
Penticton	P	British Columbia	25
Pushkino	Pu	Russia	25
Hartebeesthoek	X	South Africa	26

Table 2. The 3C 120 VLBI Observations at 5.0 and 10.7 GHz

Epoch	Frequency (GHz)	Antennas ^a	Image Peak (Jy beam ⁻¹)
1978.91	10.7	KGFO	2.07
1979.25	5.0	BGFOH	1.30
1979.44	10.7	BKGFO	0.84
1979.92	5.0	BKGFO	0.85
1980.27	10.7	BKGO	1.18
1980.52	10.7	BKGFO	1.22
1980.72	5.0	BKFO	1.51
1981.10	10.7	KGFO	0.84
1981.63	5.0	BKGYpOH	0.88
1981.93	5.0	BSKGFYpOH	1.14
1982.25	5.0	BSAGFY1OH	1.21
1982.58	5.0	BKGFYpO	0.92
1982.94	5.0	BSWJAKNGFYpO	0.83
1983.25	5.0	BAKGO	0.45 ^b
1983.57	5.0	BSKNGFYpO	0.64
1983.91	5.0	BSKGIFYpO	0.62
1984.25	5.0	BSKGFY1OH	0.53
1984.40	5.0	SMAKGFYpOH	0.48
1984.78	5.0	BSKGFYpOK	0.78
1985.12	5.0	BSAKGIFY1O	1.65
1985.41	5.0	SAKNGIY1OH	2.31
1986.42	5.0	BSAKGIFY1OH	0.89
1986.90	5.0	BSKGY1O	0.89
1987.41	5.0	BSWJMTXKGY1OH	0.84
1987.73	5.0	BSAKNGIFY1OH	0.68
1988.19	5.0	BSWJAKGIFY1O	0.56
1988.45	5.0	BSWJMKNPtY1O	0.50
1988.87	5.0	BSJMKGIFPtO	0.59

^aSee Table 1 for station codes.^bAmplitude calibration suspect for this epoch — see text.

Table 3. The 3C 120 VLBI Observations at 1.7 GHz

Epoch	Antennas ^a	Image Peak ^b (Jy beam ⁻¹)	Image RMS ^b (mJy beam ⁻¹)
1982.78	S B D J K N G A I F YpO P H	2.46	0.25
1984.26	S B W J2T E U R K N G A I F YpO P H	0.61	0.17
1989.85	S B W R PuM X J A K G I PtKpLaY1	1.50	0.21
1994.44	VLBA ^c	0.58	0.12
1997.71	B J M NtTrW G Y1 VLBA ^c	1.05	0.05

^aSee Table 1 for station codes.

^bFor the images in Figures 6 and 7.

^c“VLBA” means all 10 VLBA antennas.

Table 4. Fitted Component Speeds for Features Seen at 5 GHz

Feature	Number of Epochs	Speed ^a (mas yr ⁻¹)	Start (date)	v/c
A	4	1.47 ± 0.46	1978.22 ^{+0.28} _{-0.52}	3.00
B	13	3.14 ± 0.12	1980.38 ^{+0.07} _{-0.07}	6.39
C	5	2.17 ± 0.43	1980.73 ^{+0.27} _{-0.40}	4.41
D	10	2.72 ± 0.16	1981.86 ^{+0.08} _{-0.10}	5.53
E	6	2.40 ± 0.47	1982.56 ^{+0.19} _{-0.27}	4.88
F	5	2.41 ± 0.75	1983.31 ^{+0.34} _{-0.64}	4.90
G	3	2.42 ± 1.70	1984.27 ^{+0.43} _{-2.26}	4.93
H	3	3.37 ± 0.58	1985.74 ^{+0.18} _{-0.25}	6.86
I	7	3.20 ± 0.18	1986.10 ^{+0.10} _{-0.11}	6.51
J	6	2.23 ± 0.27	1986.59 ^{+0.17} _{-0.21}	4.53
K	3	1.45 ± 1.09	1987.56 ^{+0.49} _{-3.23}	2.96

^aThe v/c values assume $H_0 = 75$ km s⁻¹Mpc⁻¹.

Table 5. Summary of Models Discussed and Their Implications

Model	Implications Given the Observational Constraints
Simple morphological model with the particles following the apparent helix.	<p>Jet axis is very close to the line-of-sight or the brightness variations would be too large.</p> <p>Gamma is significantly higher than the minimum required for the observed superluminal motion.</p>
Physical theory focusing on the helix wavelength and the pressure distribution.	<p>Long helical wavelength implies cool external medium.</p> <p>High pressure regions and, hence, the brightest emission is to the outside of jet.</p> <p>Apparent helix from the brightest emission can have a larger radius than the helical paths followed by the particles.</p>
Simple morphological model with the apparent helix wider than the particle path helix.	<p>Allows wider angles to line of sight without excessive brightness variations.</p> <p>Gamma is near the normal value for the observed superluminal motion.</p>
Physical theory focusing on the pattern speed.	<p>Low observed pattern speed also implies cool external medium.</p> <p>Moving pattern stretches apparent helix wavelength.</p> <p>Transverse velocities are not as high as wavelength suggests.</p> <p>Constrains angle to line-of-sight to be under about 10°.</p>